Quaternion-Based Extended Kalman Filter for Determining Orientation by Inertial and Magnetic Sensing

Angelo M. Sabatini, *Senior Member, IEEE*

***Abstract*—In this paper, a quaternion based extended Kalman filter (EKF) is developed for determining the orientation of a rigid body from the outputs of a sensor which is configured as the integration of a tri-axis gyro and an aiding system mechanized using a tri-axis accelerometer and a tri-axis magnetometer. The suggested applications are for studies in the field of human movement. In the proposed EKF, the quaternion associated with the body rotation is included in the state vector together with the bias of the aiding system sensors. Moreover, in addition to the in-line procedure of sensor bias compensation, the measurement noise covariance matrix is adapted, to guard against the effects which body motion and temporary magnetic disturbance may have on the reliability of measurements of gravity and earth's magnetic field, respectively. By computer simulations and experimental validation with human hand orientation motion signals, improvements in the accuracy of orientation estimates are demonstrated for the proposed EKF, as compared with filter implementations where either the in-line calibration procedure, the adaptive mechanism for weighting the measurements of the aiding system sensors, or both are not implemented.**

***Index Terms*—Earth's magnetic field sensing, extended Kalman filter, human motion tracking, inertial sensing, quaternion.**

I. Introduction

THE DETERMINATION of position and orientation of moving objects is involved in several fields: among them, navigation of man-made vehicles and, of interest here, human motion tracking and analysis. Most motion sensing technologies in use need an external source (optical, magnetic, and acoustic) to determine location information. Usually, the source is transmitted over limited distances; interference and shadowing are additional problems associated with current technologies. Inertial sensors make it possible to determine location by measuring physical quantities (acceleration, angular velocity) which are directly related to the motion of the body part where they are placed. Being internally referenced and immune to interference and shadowing, inertial sensing can track body motion, in principle, without restrictions [1], [2].

In inertial systems, the main problem is that location is computed by time-integrating the signals from gyros and accelerometers, including any superimposed sensor drift and noise. Hence, the estimation errors tend to grow unbounded. Another drawback is that inertial sensors are not well-suited for determining absolute location: indeed, the integration has to be started from initial conditions, which inertial sensors cannot help establishing (position, velocity), or disambiguating completely (orientation). Other technologies, such as earth's magnetic field sensing, can help either mitigate the integration errors [3] or specify the absolute orientation [4]. In principle, earth's magnetic field sensing is externally referenced, although it can be used in practice as though it is internally referenced. This is because the earth's magnetic field is virtually available anywhere, and environmental modifications are not necessary to measure it.

Research is currently being carried out in many laboratories for tracking human body motion with the use of gyros, accelerometers and magnetometers. Beside the research efforts for high-grade, yet inexpensive sensors, advanced signal processing methods are intensely investigated to improve the performance of existing sensing hardware [5]. The basic idea behind complementary filtering is that orientation drift errors resulting from gyro output errors can be bounded by aiding the gyros with additional sensors, the information from which allows correcting the gyro orientation solution. The tradition of using linear Kalman filters (KFs) and their extended (EKF) version for nonlinear models is well established when complementary filters are developed to blend the outputs from gyros and the sensors of an aiding system. This is also the case when applications that require inertial sensing of human motion are considered. In this paper, an EKF is developed for estimating the orientation of a rigid body using sensor devices which are composed of one gyro, one accelerometer and one magnetometer, each of them, endowed with three perpendicular sensitive axes—henceforth, this configuration is referred to as a multi-sensor orientation determination system (MODS).

An inertial measurement unit (IMU) composed of one tri-axis accelerometer is developed in [6] for measuring inclination during dynamic tasks (gravimetric tilt sensing). Usually, accelerometers are sensitive to both gravity and bodily accelerations, which makes their discrimination difficult, especially as the speed of movement increases. The developed KF is designed to separate these components, including accelerometer bias vector, in accordance with an analytical model based on realistic assumptions about the dynamics of human movement. However, since the accelerometer signals are not affected by a rotation around the vertical, information from additional sensors is necessary to compensate for the heading drift in the proposed in-line calibration procedure.

Manuscript received March 9, 2005; revised January 5, 2006. This work was supported in part by the Fondazione Cassa di Risparmio di Pisa under the Kidrollbot Project, and in part by the Italian Ministry of University and Research.

The author is with the ARTS Lab, Scuola Superiore Sant'Anna, Piazza Martiri della Libertà, Pisa 56127, Italy (e-mail: A.Sabatini@arts.sssup.it).

Digital Object Identifier 10.1109/TBME.2006.875664

The EKF developed in [7] allows estimating the orientation of a body segment using a MODS; these authors represent the orientation with quaternions. Albeit they may suffer from problems of interpretation in terms of meaningfully clinical or anatomical angles, quaternions are interesting mathematical entities, since they require less computing time and avoid the singularity problems inherent in using other orientation descriptors, e.g., Euler angles [8], [9]. In [7], the quaternion measurement is obtained by vector matching earth's gravitational and magnetic fields, resolved by the aiding system in the body frame, with their known representation in the absolute reference frame [10]. The gyro information is integrated to track high-frequency orientation components, while quaternion measurements are used to track low-frequency components and stabilize the gyro behavior. The linearization process ensuing from vector matching by a reduced-order Gauss-Newton optimizer and the fast and robust convergence of the latter allow implementing an EKF with moderate computational overhead and good stability, although these features accrue to the filter design provided that quaternion measurements are not biased.

The adaptive EKF developed in [11] is embedded in the MODS marketed by InterSense Inc. [12]. Gravimetric tilt sensing and earth's magnetic field sensing are used for alignment and gyro stabilization; the gyro outputs are then integrated to yield the orientation changes between successive measurements. To guard against the effects of body motion, the acceleration magnitude is further tested for significant deviations from gravity [13]. If these deviations are not detected, gravimetric tilt sensing is used to correct pitch and roll drift; otherwise, the accelerometer measurements receive a lesser weighting [14]. The level of yaw compensation is specified by hand-crafting the weight of magnetic measurements during filter initialization. To guard against the effects of temporary magnetic disturbances, a screening technique similar to that described above for acceleration measurements may be based on testing the sensed magnetic field strength for significant deviations from the local earth's magnetic field strength [15], [16]. In-line calibration procedures to compensate for the bias originated from exposing the MODS to magnetically disturbed environments are not fully pursued in [11]–[15].

In this paper, we develop a quaternion based EKF with the following features: a state augmentation technique is applied in the process model and a specific measurement model is formulated, in the attempt to capture the bias vectors of both accelerometer and magnetometer (in-line calibration)—this part of the work is related to previously reported in-line calibration efforts for motion tracking and analysis in the medical field [7], [16], robotics [17], and virtual environment systems [18]; the measurement noise covariance matrix is adapted at run-time, to guard against the effects of body motion and temporary magnetic disturbances on the reliability of an aiding system sensor measurements—this part of the work is related to previous efforts to make an EKF adaptive in applications that require inertial sensing of human motion [11], [15], [16]. Because of the inherent inability of accelerometers to provide accurate heading estimates, magnetic sensing is argued to effectively complement inertial sensing for applications in the field of human body motion tracking. The main contribution of this paper is the design and testing of an orientation filter which allows the in-line calibration of aiding sensors, both accelerometers and magnetic sensors—feature which is lacking in most orientation filters we are aware of. By computer simulations and experimental validation with human hand orientation motion signals, improvements in the accuracy of orientation estimates are demonstrated, as compared with filter designs, where the in-line calibration procedures, the adaptive mechanism for weighting the aiding sensor measurements, or both are not implemented.

II. Method

A. Orientation Representation and Determination

The orientation of a rigid body in space is determined when the axis orientation of a coordinate frame attached to the body (the body frame $\mathcal{B}$) is specified with respect to an absolute coordinate system, usually named the navigation frame $\mathcal{N}$.

The transformation between the representations, relative to $\mathcal{N}$ and $\mathcal{B}$, of a 3×1 column-vector $\vec{\mathbf{x}}(t)$, whose components are generally functions of time t, is expressed as

$$\vec{\mathbf{x}}^b(t) = \mathbf{C}_n^b\left[\mathbf{q}(t)\right]\vec{\mathbf{x}}^n(t). \tag{1}$$

Henceforth, the argument t will be omitted for the sake of simplicity. The direction cosine matrix (DCM) for the transformation from $\mathcal{N}$ to $\mathcal{B}$ is given in terms of the orientation quaternion $\mathbf{q} = [\vec{\mathbf{e}}^T, q_4]^T$, as shown in (2) at the bottom of the page, where $\vec{\mathbf{e}} = [q_1, q_2, q_3]^T$ is the vector part and q_4 is the scalar part of the quaternion [8].

The rigid body angular motion obeys the vector differential equation

$$\frac{d}{dt}\mathbf{q} = \mathbf{\Omega}[\vec{\boldsymbol{\omega}}]\mathbf{q} \tag{3}$$

where

$$\mathbf{\Omega}[\vec{\boldsymbol{\omega}}] = \frac{1}{2}\begin{bmatrix}[\vec{\boldsymbol{\omega}}\times] & \vec{\boldsymbol{\omega}} \\ -\vec{\boldsymbol{\omega}}^T & 0\end{bmatrix}. \tag{4}$$

$\vec{\boldsymbol{\omega}}(t) = [p, q, r]^T$ is the angular velocity of $\mathcal{B}$ relative to $\mathcal{N}$, resolved in $\mathcal{B}$. $\vec{\mathbf{\Omega}}[\vec{\boldsymbol{\omega}}]$ is a 4×4 skew symmetric matrix and the operator

$$[\vec{\boldsymbol{\omega}}\times] = \begin{bmatrix} 0 & -r & q \\ r & 0 & -p \\ -q & p & 0\end{bmatrix} \tag{5}$$

represents the standard vector cross-product [7].

$$\mathbf{C}_n^b(\mathbf{q}) = \frac{1}{\sqrt{\|\vec{\mathbf{e}}\|^2 + q_4^2}} \cdot \begin{bmatrix} q_1^2 - q_2^2 - q_3^2 + q_4^2 & 2(q_1q_2 + q_3q_4) & 2(q_1q_3 - q_2q_4) \\ 2(q_1q_2 - q_3q_4) & -q_1^2 + q_2^2 - q_3^2 + q_4^2 & 2(q_2q_3 + q_4q_1) \\ 2(q_1q_3 + q_2q_4) & 2(q_2q_3 - q_4q_1) & -q_1^2 - q_2^2 + q_3^2 + q_4^2 \end{bmatrix} \tag{2}$$

The discrete-time model corresponding to (3) is

$$\begin{cases} \mathbf{q}_{k+1} = \exp(\mathbf{\Omega}_k T_s)\mathbf{q}_k, \quad k = 0, 1, \dots \\ \mathbf{q}_0 = \mathbf{q}(0) \end{cases} \tag{6}$$

where T_s is the system sampling interval. The quaternion is determined at time instants kT_s, starting from initial conditions $\mathbf{q}_0$ that are assumed to be known or measurable during alignment. The validity of (6) is subject to the assumption that the angular velocity $\vec{\boldsymbol{\omega}}_k$ measured at time instants kT_s is constant in the interval $[kT_s, (k+1)T_s]$. Equation (2) is used to update the DCM expression, once that the solution of (6) has progressed in time.

B. Sensor Model

The gyro, the accelerometer and the magnetometer are sensor triplets with perpendicular sensitivity axes. Their output in response to the angular velocity $\vec{\boldsymbol{\omega}}_{\text{true}}$, total acceleration (gravity $\vec{\mathbf{g}}$ and acceleration $\vec{\mathbf{a}}_{\text{body}}$), earth's magnetic field $\vec{\mathbf{h}}$ are expressed, respectively, by

$$\begin{cases} \vec{\boldsymbol{\omega}} = {}^{g}\mathbf{K}\vec{\boldsymbol{\omega}}_{\text{true}} + {}^{g}\vec{\mathbf{b}} + {}^{g}\vec{\mathbf{v}} \\ \vec{\mathbf{a}} = {}^{a}\mathbf{K}\left[\mathbf{C}_n^b(\mathbf{q})(\vec{\mathbf{g}} + \vec{\mathbf{a}}_{\text{body}})\right] + {}^{a}\vec{\mathbf{b}} + {}^{a}\vec{\mathbf{v}} \\ \vec{\mathbf{m}} = {}^{m}\mathbf{K}\mathbf{C}_n^b(\mathbf{q})\vec{\mathbf{h}} + {}^{m}\vec{\mathbf{b}} + {}^{m}\vec{\mathbf{v}} \end{cases} \tag{7}$$

where ${}^{g}\mathbf{K}$, ${}^{a}\mathbf{K}$, and ${}^{m}\mathbf{K}$ are the scale factor matrices (ideally, they are equal to the 3×3 identity matrix $\mathbf{I}$); ${}^{g}\vec{\mathbf{b}}$, ${}^{a}\vec{\mathbf{b}}$, and ${}^{m}\vec{\mathbf{b}}$ are the bias vectors (ideally, they are null); ${}^{g}\vec{\mathbf{v}}$, ${}^{a}\vec{\mathbf{v}}$, and ${}^{m}\vec{\mathbf{v}}$ are assumed uncorrelated white Gaussian measurement noise, with null mean and covariance matrix $\mathbf{\Sigma}_g = \sigma_g^2\mathbf{I}$, $\mathbf{\Sigma}_a = \sigma_a^2\mathbf{I}$, and $\mathbf{\Sigma}_m = \sigma_m^2\mathbf{I}$. Equation (7) is a simplified model which does not account for cross-axis sensitivity, cross-coupling, and misalignment [16], [19]–[21].

The bias and scale factor of inertial sensors are functions of environmental conditions, in particular the ambient temperature; this is especially true for gyros, while the temperature coefficients of accelerometers are of relatively lower quantitative relevance and the temperature coefficients of magnetometers have insignificant effects on their behavior across the temperature variations that they may encounter in practice [17], [22]. Moreover, scale factor drifts of inertial sensors are known to affect the accuracy of the measurement process to a much lesser extent than the bias drifts of these sensors [1]. In the case of gyros, temperature variations are considered the most important element to determine the bias drift. The bias drift is significant especially after power is applied to gyros, as a result of device self-heating [22]. Provided that gyros are allowed warm-up and thermal stabilization for few minutes, then their biases tend to change quite slowly with time.

Henceforth, we assume that scale factor and bias errors of gyros in (7a) are constant; in practice, bias errors can be calibrated and compensated effectively by bias capture procedures based on so-called "zero attitude updates," which require keeping the gyros from rotating [23], [24]. As for the accelerometer, we assume that scale factor and bias error in (7b) are constant; in practice, bias errors can be calibrated and compensated effectively, although the bias capture procedures based on so-called "zero velocity updates", which require keeping the accelerometers from moving as described in [25], are more difficult to implement and may require specific maneuvers to work properly [6], [26]. Zero attitude or velocity updates may rely on the stereotypical feature of human movements to alternate movements of limb segments, the rotation of which can be measured using gyros, with rest periods, in preparation for the next movement of these segments. It is indeed during these rest periods that the aiding sensors can be used to compute the initial conditions from which the gyro integration will start [23], [24]. It would also be important to detect these rest periods in order to dynamically reset the gyro outputs. Henceforth, a zero attitude update, similar to the one implemented in [24], is performed just at the beginning of each simulated and experimental run.

Usually, the magnetometer error is described by taking into account the effects of so-called hard irons and soft irons [3]. Hard iron errors are those due to unwanted fields, either stationary or time-varying, that are generated by ferromagnetic materials nearby the magnetometer. The effect of their superposition to the sensed earth's magnetic field is to bias the magnetometer output [16]. Soft iron errors are due to the fields which, in response to externally applied fields, are generated by some materials, which include clothes and accessories worn by the person carrying the magnetometer [15]. In response to the earth's magnetic field, soft irons generate a magnetic field that will be superimposed on the magnetometer output. Since the orientation of the earth's magnetic field vector relative to the soft irons change during unrestrained movements, the resulting effect on the magnetic field is highly complex, and would not be easily modeled. However, because of the strong dependence of parasitic magnetic fields on the distance from the source, the impact of either hard or soft irons, e.g., mobile phones, can be minimized taking care during sensor placement. The automatic procedure of in-line calibration is intended to detect and correct situations when the deviation in the compass is produced by external magnetic interference which act in the sense to bias the magnetometer output: while hard irons tend to act as static bias vectors, the effects of either static or time-varying external magnetic interferences are modeled as trajectory-dependent time-varying bias vectors. Finally, since the objective here is to get a reference orientation from the MODS within a relatively small tracking area, the errors due to the difference between the compass reading and the geographic north direction on earth, i.e., variation and declination [3], are not considered in the sensor model (7c).

C. Filter Design

The state vector is composed of the rotation quaternion, augmented by the tri-axis accelerometer and magnetometer bias vectors, the components of which are modeled as random walk. The state transition vector equation is

$$\begin{aligned} \vec{\mathbf{x}}_{k+1} &= \begin{bmatrix} \mathbf{q}_{k+1} \\ {}^{a}\vec{\mathbf{b}}_{k+1} \\ {}^{m}\vec{\mathbf{b}}_{k+1} \end{bmatrix} = \Phi(T_s, \vec{\boldsymbol{\omega}}_k)\vec{\mathbf{x}}_k + \vec{\mathbf{w}}_k \\ &= \begin{bmatrix} \exp(\mathbf{\Omega}_k T_s) & \mathbf{0} & \mathbf{0} \\ \mathbf{0} & \mathbf{I} & \mathbf{0} \\ \mathbf{0} & \mathbf{0} & \mathbf{I} \end{bmatrix} \begin{bmatrix} \mathbf{q}_k \\ {}^{a}\vec{\mathbf{b}}_k \\ {}^{m}\vec{\mathbf{b}}_k \end{bmatrix} + \begin{bmatrix} {}^{q}\vec{\mathbf{w}}_k \\ {}^{a}\vec{\mathbf{w}}_k \\ {}^{m}\vec{\mathbf{w}}_k \end{bmatrix} \end{aligned} \tag{8}$$

where $\mathbf{0}$ is the 3×3 null matrix and

$$ {}^{q}\vec{\mathbf{w}}_k = -\frac{T_s}{2}\mathbf{\Xi}_k {}^{g}\vec{\mathbf{v}}_k = -\frac{T_s}{2}\begin{bmatrix} [\vec{\mathbf{e}}_k\times] + q_{4k}\mathbf{I} \\ -\vec{\mathbf{e}}_k^T \end{bmatrix} {}^{g}\vec{\mathbf{v}}_k. \quad (9) $$

${}^{a}\vec{\mathbf{w}}_k$ and ${}^{m}\vec{\mathbf{w}}_k$ are zero-mean white noise processes, with covariance matrix ${}^{a}\mathbf{\Sigma}_k = T_s^a \sigma_w^2 \mathbf{I}$ and ${}^{m}\mathbf{\Sigma}_k = T_s^m \sigma_w^2 \mathbf{I}$, respectively. The part of the sensor model in (8), (9) describing the quaternion time-evolution is a first-order approximation in ${}^{g}\vec{\mathbf{v}}_k$ and T_s of the exact process (6) [27]. Underlying this approximation is the consideration that the true angular velocity vector to be used in (6) is not known in practice, but it is rather measured. The gyro measurement noise vector ${}^{g}\vec{\mathbf{v}}_k$ is assumed small enough that a first order approximation of the "noisy" transition matrix is possible, yielding (9). Because of the assumption that ${}^{q}\vec{\mathbf{w}}_k$, ${}^{a}\vec{\mathbf{w}}_k$ and ${}^{m}\vec{\mathbf{w}}_k$ are not correlated with one another, the process noise covariance matrix $\mathbf{Q}_k$ will have the following expression:

$$ \mathbf{Q}_k = \begin{bmatrix} (T_s/2)^2 \mathbf{\Xi}_k \mathbf{\Sigma}_g \mathbf{\Xi}_k^T & \mathbf{0} & \mathbf{0} \\ \mathbf{0} & {}^{a}\mathbf{\Sigma}_k & \mathbf{0} \\ \mathbf{0} & \mathbf{0} & {}^{m}\mathbf{\Sigma}_k \end{bmatrix}. \quad (10) $$

The measurement model is constructed by stacking the accelerometer and magnetometer measurement vectors

$$ \begin{aligned} \vec{\mathbf{z}}_{k+1} &= \begin{bmatrix} \vec{\mathbf{a}}_{k+1} \\ \vec{\mathbf{m}}_{k+1} \end{bmatrix} = \mathbf{f}[\vec{\mathbf{x}}_{k+1}] + \vec{\mathbf{v}}_{k+1} \\ &= \begin{bmatrix} \mathbf{C}_n^b(\mathbf{q}_{k+1}) & \mathbf{0} \\ \mathbf{0} & \mathbf{C}_n^b(\mathbf{q}_{k+1}) \end{bmatrix} \begin{bmatrix} \vec{\mathbf{g}} \\ \vec{\mathbf{h}} \end{bmatrix} \\ &\quad + \begin{bmatrix} {}^{a}\vec{\mathbf{b}}_{k+1} \\ {}^{m}\vec{\mathbf{b}}_{k+1} \end{bmatrix} + \begin{bmatrix} {}^{a}\vec{\mathbf{v}}_{k+1} \\ {}^{m}\vec{\mathbf{v}}_{k+1} \end{bmatrix}. \end{aligned} \quad (11) $$

The covariance matrix of the measurement model $\mathbf{R}_{k+1}$ is

$$ \mathbf{R}_{k+1} = \begin{bmatrix} {}^{a}\mathbf{R}_{k+1} & \mathbf{0} \\ \mathbf{0} & {}^{m}\mathbf{R}_{k+1} \end{bmatrix}. \quad (12) $$

Underlying (12) is the assumption that the accelerometer and magnetometer measurement noise ${}^{a}\vec{\mathbf{v}}_{k+1}$ and ${}^{m}\vec{\mathbf{v}}_{k+1}$ are uncorrelated zero-mean white noise processes, the covariance matrices of which are ${}^{a}\mathbf{R}_{k+1} =^R \sigma_a^2 \mathbf{I}$ and ${}^{m}\mathbf{R}_{k+1} =^R \sigma_m^2 \mathbf{I}$, respectively.

Before the current measurement $\vec{\mathbf{z}}_{k+1}$ is incorporated in the filtering process to drive the state vector update, a mechanism of adaptation of the measurement noise covariance matrix is implemented. The part of (11) which describes the accelerometer measurement model differs from the sensor model (7b) in that the acceleration component related to body motion cannot be present. In our approach, the measured acceleration magnitude is tested in advance for the absence of significant deviations from gravity [11], [13], [14]; if persistent for some specified time interval, this absence is considered the sign that the body is at rest. If not so, the observation variance ${}^{R}\sigma_a^2$ is set to extremely high values, so as to force the filter to rely on the magnetic information for carrying the state vector update [14]

$$ {}^{R}\sigma_a^2 = \begin{cases} \sigma_a^2, & \left| \|\vec{\mathbf{a}}_{j+1}\| - \|\vec{\mathbf{g}}\| \right| < \varepsilon_a \ \ \forall j \in [k - k_a, k] \\ \infty, & \text{otherwise} \end{cases}. \quad (13) $$

In magnetically perturbed environments, the deviation of the sensed magnetic field magnitude from the local earth's magnetic field magnitude can be so large, and the dip angle, namely the angle formed by the earth's magnetic field relative to the horizontal

$$ \hat{\theta}_{\text{dip}} = \arccos\left(\frac{\mathbf{C}_b^n\left(\mathbf{q}_{k+1}^-\right) \vec{\mathbf{m}}_{k+1} \cdot \mathbf{C}_b^n\left(\mathbf{q}_{k+1}^-\right) \vec{\mathbf{a}}_{k+1}^-}{\|\vec{\mathbf{m}}_{k+1}\| \left\|\vec{\mathbf{a}}_{k+1}^-\right\|} \right) \quad (14) $$

can deviate so much from the local value θ_{dip}, to raise a serious concern about the reliability of the magnetic information [14]; the term $\mathbf{C}_b^n(\mathbf{q}_{k+1}^-)\vec{\mathbf{a}}_{k+1}^-$ in (14) is the predicted gravity (The superscript—stands for "*a priori* estimate at time t_{k+1}, before the current measurement $\vec{\mathbf{z}}_{k+1}$ is used in the computation of the *a posteriori* estimate" [28]). The following validation test is implemented:

$$ {}^{R}\sigma_m^2 = \begin{cases} \sigma_m^2, & \left| \|\vec{\mathbf{m}}_{k+1}\| - \|\vec{\mathbf{h}}\| \right| < \varepsilon_m \cap \left| \hat{\theta}_{\text{dip}} - \theta_{\text{dip}} \right| < \varepsilon_{\text{dip}} \\ \infty, & \text{otherwise} \end{cases}. \quad (15) $$

Rather than dealing with acceleration and magnetic disturbances as time-varying components of the bias vectors, the proposed validation tests aim at precluding the measurements from influencing the filter behavior, when detected disturbances are characterized by high magnitude or duration. In this regard, the tests implement a sort of gating technique, which can be used alone, as in the present filter design, or in combination eventually with any of the gating techniques reported in the literature on Kalman filters [28].

Because of the nonlinear nature of (11), the EKF approach requires that a first-order Taylor-Mac Laurin expansion is carried out around the current state estimate by computing the Jacobian matrix:

$$ \mathbf{F}_{k+1} = \left. \frac{\partial}{\partial \vec{\mathbf{x}}_{k+1}} \bar{\vec{\mathbf{z}}}_{k+1} \right|_{\vec{\mathbf{x}}_{k+1} = \vec{\mathbf{x}}_{k+1}^-}. \quad (16) $$

As an example, the element $\mathbf{F}_{k+1}(1,1)$ is given by

$$ \mathbf{F}_{k+1}(1,1) = \frac{1}{\sqrt{\|\vec{\mathbf{e}}\|^2 + q_4^2}} \begin{bmatrix} 2q_1 - \mathbf{C}_n^b(1,1)q_1 \\ 2q_2 - \mathbf{C}_n^b(1,2)q_1 \\ 2q_3 - \mathbf{C}_n^b(1,3)q_1 \end{bmatrix}^T \cdot \vec{\mathbf{h}}. \quad (17) $$

As it is evident from inspection of (8)–(11), the statistical models which are considered in this EKF development are state-dependent. However, the expression of the true state is not known; it is common practice to handle this dependence by substituting the best estimate of the state available, namely the *a priori* state estimate, instead of the true state. Another subtle detail is in the use of the quaternion as part of the state vector. Since, to represent a valid rotation, a quaternion must have unit-norm, the four quaternion components are interdependent. Although the state transition matrix $\Phi(T_s, \vec{\boldsymbol{\omega}}_k)$ is orthogonal, the unit-norm property of the *a posteriori* quaternion must be preserved by a normalization step, which is common practice to perform by dividing it by its Euclidean norm [27].

For the sake of reader's convenience, the EKF equations are summarized below [28].

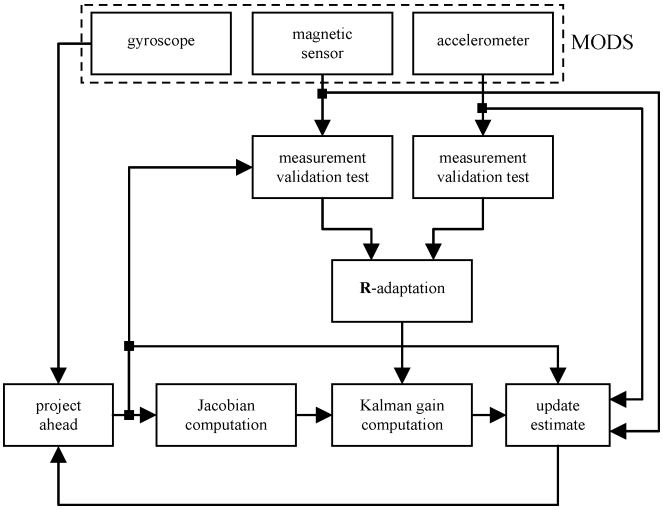

Fig. 1. EKF structure. The block "project ahead" computes the *a priori* state estimate and error covariance matrix. The DCM estimation is also carried within this block, and used to implement the measurement validation test (13), see (14), and to compute the Jacobian matrix, see (16), (17), which is also needed for updating the expression of the Kalman gain. The block "update estimate" computes the *a posteriori* state estimate and error covariance matrix. The measurement validation tests implement (13)–(15), in preparation for the adaptation of the measurement noise covariance matrix, see (12). The iterative nature of the discrete-time EKF allows exploiting the statistics available at the k-th time-step to start the computations at the next time-step, when a new set of measurements from the MODS sensors becomes available.

- Compute the *a priori* state estimate

$$\vec{\mathbf{x}}_{k+1}^{-} = \Phi(T_s, \vec{\boldsymbol{\omega}}_k)\vec{\mathbf{x}}_k.$$

- Compute the *a priori* error covariance matrix

$$\mathbf{P}_{k+1}^{-} = \Phi(T_s, \vec{\boldsymbol{\omega}}_k)\mathbf{P}_k\Phi(T_s, \vec{\boldsymbol{\omega}}_k)^T + \mathbf{Q}_k.$$

- Compute the Kalman gain

$$\mathbf{K}_{k+1} = \mathbf{P}_{k+1}^{-}\mathbf{F}_{k+1}^T\left(\mathbf{F}_{k+1}\mathbf{P}_{k+1}^{-}\mathbf{F}_{k+1}^T + \mathbf{R}_{k+1}\right)^{-1}.$$

- Compute the *a posteriori* state estimate

$$\vec{\mathbf{x}}_{k+1} = \vec{\mathbf{x}}_{k+1}^{-} + \mathbf{K}_{k+1}\left[\vec{\mathbf{z}}_{k+1} - \mathbf{f}\left(\vec{\mathbf{x}}_{k+1}^{-}\right)\right].$$

- Compute the *a posteriori* error covariance matrix

$$\mathbf{P}_{k+1} = \mathbf{P}_{k+1}^{-} - \mathbf{K}_{k+1}\mathbf{F}_{k+1}\mathbf{P}_{k+1}^{-}.$$

The flow-chart of computations performed by the proposed EKF is summarized in Fig. 1.

D. Computer Simulations

One data-set of human hand orientation motion was used in our study as a representative example of human motion dynamics which may be frequently encountered during daily-life functional activities. The data-set, called HAND set henceforth, was acquired from an InertiaCube2 orientation sensor (InterSense Inc., Burlington, MA), interfaced to a PC via a serial communication interface (RS232 communication protocol, baud rate: 115 200 bps), [12].

TABLE I
VALUES OF BIAS, SENSITIVITY, AND MEASUREMENT NOISE STANDARD DEVIATION USED TO SIMULATE THE SENSOR BEHAVIOR. THESE VALUES WERE TYPICAL OF THE CALIBRATION RESULTS OBTAINED WHEN AN INERTIACUBE2 ORIENTATION SENSOR WAS SUBMITTED TO STANDARD CALIBRATION PROCEDURES IN OUR LAB

	Sensitivity	Bias	Standard deviation
Gyro	[1.05 1.05 1.05]	[2.5 2.5 2.5] (mrad/s)	[10 10 10] (mrad/s)
Accelerometer	[1.01 1.01 1.01]	[0.25 0.25 0.25] (m/s^2)	[5e-2 5e-2 5e-2] (m/s^2)
Magnetometer	[1.04 1.01 0.99]	[60 20 -30] (mGauss)	[1 1 1] (mGauss)

To construct the HAND set, the tracking device was snugly strapped to the subject's wrist using a Velcro strap. In the initial posture, the subject was seated at a distance of about 40 cm from a table, the palm of the instrumented hand lying on the thigh; the MODS sensitive axes were aligned with the body axes: sagittal, frontal, and longitudinal. The subject was asked to move the arm at freely selected speed, as though he had to laterally reach a target area on the tabletop with the wrist rotated about 90°, then to move the hand to the mouth in the attempt to mimic drinking, before back-tracing the hand path to the initial posture. The recorded movement lasted about 18 s. The time functions of the quaternion components were delivered by the InertiaCube2 at a sampling rate of 100 Hz. Data were off-line processed using Matlab v. 6.0.

The truth reference data-set for algorithm testing was obtained from filtering the quaternion components with a second-order forward-backward low-pass Butterworth filter (cut-off frequency: 5 Hz).

Standard conversion formulas allowed constructing the orientation vector $\vec{\boldsymbol{\varphi}}$; its time-derivative $\dot{\vec{\boldsymbol{\varphi}}}$ was obtained by applying the central difference technique to the orientation vector samples. $\vec{\boldsymbol{\varphi}}$ and $\dot{\vec{\boldsymbol{\varphi}}}$ were used to estimate the angular velocity vector that generated that specified orientation as stated in [29]. The sensed gravitational and magnetic fields were computed from resolving gravitational and geomagnetic fields—$\vec{\mathbf{g}} = [0\ 0\ \mathrm{g}]^T$ ($g = 9.81\ \mathrm{m/s^2}$) and $\vec{\mathbf{h}} = [h_x\ 0\ \mathrm{h_z}]^T$, respectively—into the body frame via the estimated DCM.

The sensor orientation was not referred to the true magnetic or geographic north; instead yaw was estimated relative to the initial hand posture. Before moving, the hand was at rest for few seconds, so as to estimate the earth's magnetic field in conditions of null yaw. Random Gaussian noise was injected into the sensor time functions to simulate the effect of specified amounts of measurement noise.

For the purpose of algorithm testing, the time interval [0, 18] s was divided in four subintervals: the subinterval $T_1 = [0, 5]\,\mathrm{s}$, where perfectly calibrated sensors were simulated; in the other subintervals, namely $T_2 = [5, 10]\ \mathrm{s}$, $T_3 = [10, 13.25]\ \mathrm{s}$, and $T_4 = [13.25, 18]\ \mathrm{s}$, sensor bias and scale factor were set to values different from initial calibration setting, Table I.

The conditions within the subinterval T_3 were further modified by introducing motion and magnetic disturbances: the

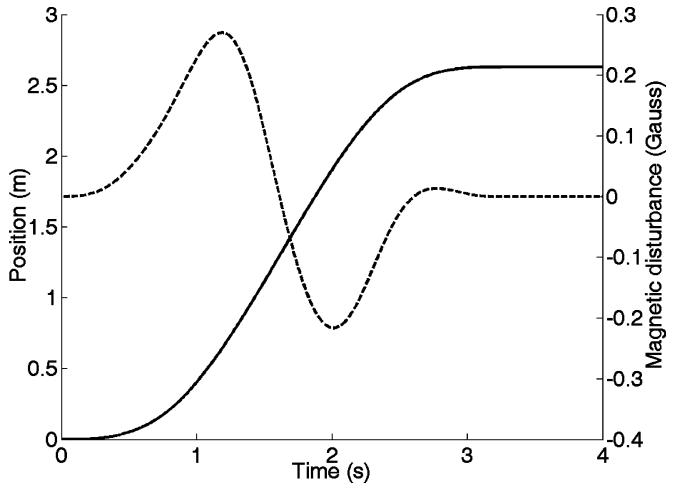

Fig. 2. The displacement of the body frame origin which occurs in the local level plane is responsible for a linear acceleration component the magnitude of which is up to 2 $\mathrm{m/s^2}$ (solid line). The dipole-like magnetometer disturbance is oriented in the direction of the local earth's magnetic field, as though a metallic mass is moving nearby the magnetometer (dashed line).

sensor was linearly displaced in a plane perpendicular to gravity at a time when it was also exposed to a time-varying magnetic field, oriented in the direction of the earth's field, Fig. 2.

Four EKF implementations were studied, henceforth called Method A, B, C, and D. Method A and Method B incorporated the in-line calibration of the aiding system sensors; Method A adapted the measurement noise covariance matrix $\mathbf{R}$, while Method B did not adapt it. Method C and Method D did not incorporate the in-line calibration of the aiding system sensors; Method C adapted $\mathbf{R}$, while Method D did not adapt it. Filter initialization was performed by gravimetric tilt and earth's magnetic field sensing at first contact. An additional method, called Method E, was based on quaternion time-propagation by integrating (6) from initial conditions which were externally provided to the algorithm. The five methods were tested at three different sampling rates: 100 Hz, 50 Hz, and 25 Hz. Ten Monte Carlo trials were conducted for each condition (method and sampling rate). In the simulations concerning the performance assessment of Method A and Method C, $\varepsilon_a = 0.2\ \mathrm{m/s^2}$, $\varepsilon_m = 0.1$ Gauss, $\varepsilon_{\mathrm{dip}} = 10°$, and $k_a T_s = 0.1$ s.

The performance metrics were based on computing $\Delta\mathbf{q} = \mathbf{q}_{\mathrm{true}}^{-1} \otimes \mathbf{q}$, where $\mathbf{q}_{\mathrm{true}}$ and $\mathbf{q}$ were truth-reference and estimated quaternions, respectively. The quaternion $\Delta\mathbf{q}$ represented the rotation which brought the estimated body frame onto $\mathcal{B}$. The orientation error was obtained from the scalar component of $\Delta\mathbf{q}$: $\Delta\theta = 2\arccos(\Delta q_4)$. The performance metrics were given by the root-mean-square error (RMSE_θ) of $\Delta\theta$, computed over the four subintervals.

E. Experimental Validation

The experimental validation was carried out in the course of an experiment which consisted of moving a plastic plate, raised from ground, by hand, at freely selected speed for 120 s within a measurement space of about $60\times60\times60\ \mathrm{cm^3}$. The InertiaCube2 was placed on top of the plate and fastened using double-side adhesive tape. As a truth reference, the plate orientation was recorded using a nine-camera Vicon optical motion capturing system with a sampling rate of 100 Hz. The system measured the position of three reflective markers (diameter: 14 mm) arranged to form an equilateral triangle on top of the plate (triangle side: 20 cm); an additional marker was placed on top of the InertiaCube2 (not used here). This configuration allowed constructing a marker frame, the accuracy of which was obtained by analyzing the relative motion of two markers. The RMS of the Vicon orientation error was assumed to be in the same order as the RMS distance variation divided by the distance between two markers.

The basic idea behind orientation determination using the Vicon system was the fact that three noncollinear points in space define a plane, the orientation of which could be easily computed relative to the predefined reference frame. The corresponding roll, pitch, and yaw time functions computed from the position data provided by Vicon were considered the truth reference for the purpose of error estimation. The orientation of the sensor frame relative to the marker frame was found by holding the plate still for few seconds at the beginning of the trial, so as to compute the calibration quaternion which brought the sensor frame into coincidence with the marker frame. Gyro bias capture was done during heading reset. The quaternions produced by Method A—the context winner of the simulation runs—and Method E were converted in Euler angles using standard conversion formulas. The time functions of the roll, pitch and yaw estimation errors were off-line constructed by computing the difference between the roll, pitch, and yaw estimates produced by each tested filtering algorithm and the truth reference. Hence, beside the RMSE_θ value, RMSEs of roll, pitch and yaw estimates were computed using three different approaches: Method A, Method E, and the native InertiaCube2 filtering algorithm (default parameter initialization), henceforth named Method F.

III. Results

The quaternion time functions of the HAND data-set are shown in Fig. 3.

To process the HAND data-set noisy sensor data, constructed as stated in Section II-D, the filter parameters are those indicated in Table II.

The statistics of the orientation RMSE_θ are reported in Tables III and IV. The results in Table IV are obtained by setting values of the random walk model parameters which achieve the best performance after extensive testing when the simulation is carried out in the absence of motion and magnetic disturbances (this optimal filter parameter initialization is shown in Table II as row A1–A2).

Figs. 5–7 show the time functions of the Euler angles as they are measured from the Vicon system during the experimental validation trial, together with the corresponding error time functions produced by Method A. The RMS of the Vicon orientation error is almost the same for roll, pitch and yaw, and turns out to have, in this experiment, a standard deviation (SD) of about 0.4°. Typical errors made by Method A in estimating the quaternion components are sketched in Fig. 4 (motion and magnetic disturbances not inserted in the subinterval T_3; optimal filter parameter initialization).

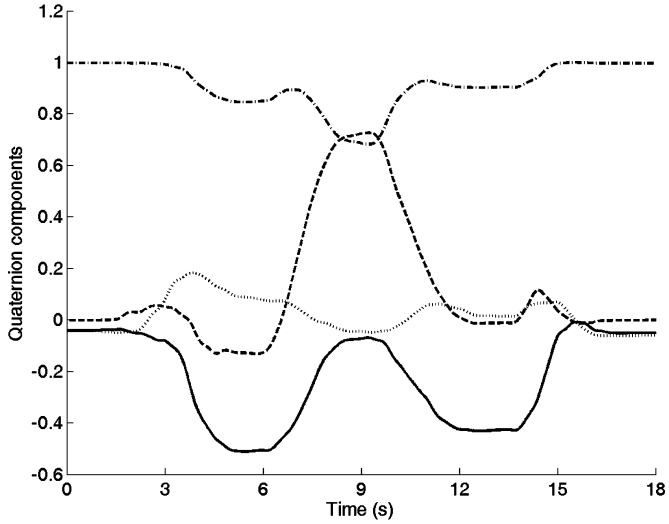

Fig. 3. The four time functions related to the unit-norm quaternion of rotation from the HAND data-set. The quaternion components are dimensionless. First component: solid line; second component: dotted line; third component: dashed line; fourth component: dash-dot line.

TABLE II
FILTER PARAMETER INITIALIZATION

	σ_g [mrad/s]	σ_a [m/s^2]	σ_m [mGauss]	${}^a\sigma_w$ [m/s^2]	${}^m\sigma_w$ [mGauss]
A	100	5e-2	1	5e-1	50
B	100	5e-2	1	1	100
C	100	4e-1	8	–	–
D	100	4e-1	8	–	–
A1-A2	100	5e-2	1	1e-1	10
A (exp.)	100	1e-1	2	5e-1	50

The filter parameter initialization for Method A is included in Table II as row A (experimental). The accuracy of the methods tested during the experimental validation trial is reported in Table V.

IV. DISCUSSION AND CONCLUSION

The simulation trials are assumed to start with perfectly calibrated sensors, namely unit scale factor and null bias. The values of the sensor model parameters in Table I, which are enforced from time $t = 5$ s on in the simulations, are typical of the range of values obtained by calibrating the InertiaCube2 in different parts of a laboratory room using the procedures described in [19] and [20].

Zero attitude and velocity updates are not implemented in the simulation runs to perform gyro and accelerometer bias capture. Since gyro bias is defined as the output produced by gyros at rest, bias can be estimated anytime the gyro is detected to be at rest: it should be pointed out that it is a stereotypical feature of most human motions to exhibit rest periods of some duration, at almost regular time intervals, e.g., walking [24], or sporadically, e.g., as during hands or head movements, which makes gyro calibration and compensation by zero attitude update quite effective and simple. As for the accelerometer, bias capture procedures use zero velocity updates, which require keeping the accelerometers from moving. The in-line calibration procedure described in [26] is an interesting variant of zero velocity updates, where a tri-axis accelerometer is exposed to the influence of gravity in several static orientations in order to estimate accelerometer bias. The in-line procedure of bias compensation is embedded in the improved EKF to perform this compensation automatically.

It should be pointed out that an element of complication in the performance analysis of a filtering algorithm for inertial navigation is the effect that the sensed trajectory may have on its behavior: certain errors of the inertial sensors are in fact trajectory-dependent, e.g., scale factor errors [22]. Rather than on a wide variety of trajectories in the three-dimensional space, the methods described in this paper are exercised on a synthetic trajectory [21]; because of the way it is constructed, the synthetic trajectory sketched in Fig. 3 in quaternion space is intended to replicate important features of human hand orientation motion dynamics.

The filter parameter initialization reported in Table II is found to work well after running an extensive number of tests in the presence of the simulated disturbances. Of course, for different trajectories and time-varying disturbances, different sets of filter parameters would be probably better. In general, it should be outlined the important role played by the process noise covariance matrix in tailoring the EKF responsiveness. A good rule of thumb is to increase the process noise in the effort to compensate for the disturbing effects of inaccurate modeling and to improve the tracking ability of the filtering algorithm [28]. Of course, this may be at the expense of the estimation accuracy when "calmness is restored." In our implementation the quite high value of the gyro measurement SD is entered in the process noise covariance matrix to counteract the effects of gyro imperfect calibration. The SD assumed for the random walk model which describes the time-evolution of the accelerometer and magnetometer bias vectors must also be sufficiently large: a careful look at the sensor model (7) shows that the effect of scale factor errors and constant null-shift errors is to produce measurement errors which look like trajectory-dependent temporary bias errors. If the in-line compensation procedure is disabled, the natural thing to do is to increase the SDs in the measurement noise covariance matrix, see the filter parameter initialization in Table II used for Method C and D; the latter means that the *a priori* state estimates, which are driven by gyro measurements, as indicated in (8) and (9), are assumed to be more reliable than the measurements from the sensors of the aiding system.

The results reported in Table III show that it is the combination of in-line bias compensation and adaptation of the measurement noise covariance matrix to give the best performance. The measurement validation tests detect the presence of a time-varying disturbance with some delay, dependent on both the disturbance rise time and the threshold setting. In spite that disturbance spectral components may generally have somewhat higher-frequency content than human motion quaternion components, the need to prevent frequent false alarms forces to choose threshold values in (13) and (15) which cannot be too low. Before time-varying disturbances are detected, the linearization procedure within the EKF is, thus, susceptible to

TABLE III
ORIENTATION ESTIMATE RMSE (°)—MEAN ±SD—PRODUCED BY THE DIFFERENT FILTERING METHODS IN THE COURSE OF THE MONTE CARLO PERFORMANCE ANALYSIS. THE FILTER PARAMETER INITIALIZATION IS THAT REPORTED IN Table II. THE ACCELEROMETER AND MAGNETOMETER DISTURBANCES ARE INTRODUCED WITHIN THE INTERVAL T3, SEE TEXT

	T_1	T_2	T_3	T_4
f_s = 100 Hz				
A	0.22 ± 0.05	3.32 ± 0.08	3.52 ± 0.05	1.75 ± 0.12
B	0.24 ± 0.05	3.62 ± 0.08	3.77 ± 0.08	4.03 ± 0.14
C	0.13 ± 0.01	2.95 ± 0.01	20.76 ± 0.10	3.90 ± 0.02
D	0.13 ± 0.01	2.95 ± 0.01	27.36 ± 0.08	3.81 ± 0.02
E	0.27 ± 0.06	4.04 ± 0.09	3.19 ± 0.12	3.86 ± 0.15
f_s = 50 Hz				
A	0.34 ± 0.08	3.38 ± 0.16	4.12 ± 0.14	2.53 ± 0.32
B	0.37 ± 0.08	3.65 ± 0.18	3.88 ± 0.19	4.12 ± 0.28
C	0.18 ± 0.02	3.12 ± 0.03	20.90 ± 0.05	4.00 ± 0.03
D	0.18 ± 0.02	3.12 ± 0.03	26.31 ± 0.08	4.12 ± 0.03
E	0.43 ± 0.09	4.07 ± 0.21	3.38 ± 0.27	3.93 ± 0.34
f_s = 25 Hz				
A	0.47 ± 0.06	3.26 ± 0.13	4.57 ± 0.17	3.03 ± 0.33
B	0.53 ± 0.07	3.56 ± 0.15	4.17 ± 0.21	4.34 ± 0.30
C	0.25 ± 0.02	3.31 ± 0.04	21.30 ± 0.31	4.18 ± 0.05
D	0.25 ± 0.02	3.31 ± 0.04	26.65 ± 0.32	4.46 ± 0.06
E	0.62 ± 0.08	4.00 ± 0.18	3.80 ± 0.31	4.10 ± 0.36

TABLE IV
ORIENTATION ESTIMATE RMSE (°)—MEAN ± SD—PRODUCED BY METHOD A, EITHER IN THE ABSENCE OF SIMULATED MOTION AND MAGNETIC DISTURBANCES (A1) OR IN THEIR PRESENCE (A2)

	T_1	T_2	T_3	T_4
f_s = 100 Hz				
A1	0.19 ± 0.03	2.56 ± 0.04	1.25 ± 0.04	0.91 ± 0.04
A2	0.19 ± 0.03	2.56 ± 0.04	7.52 ± 0.09	3.54 ± 0.08
f_s = 50 Hz				
A1	0.26 ± 0.04	2.60 ± 0.09	1.40 ± 0.09	1.00 ± 0.14
A2	0.26 ± 0.04	2.60 ± 0.09	12.11 ± 0.05	3.72 ± 0.22
f_s = 25 Hz				
A1	0.32 ± 0.04	2.47 ± 0.07	1.44 ± 0.10	1.04 ± 0.13
A2	0.32 ± 0.04	2.47 ± 0.07	12.00 ± 0.10	4.10 ± 0.36

TABLE V
QUATERNION ORIENTATION, ROLL, PITCH, AND YAW ESTIMATION RMSE (°), PRODUCED BY METHOD A, METHOD E, AND METHOD F (EXPERIMENTAL VALIDATION)

	A	E	F
RMSE	4.57	9.01	7.03
$RMSE_{roll}$	1.31	3.98	1.01
$RMSE_{pitch}$	1.40	8.13	1.19
$RMSE_{yaw}$	4.13	2.06	6.93

induce undesirable effects such as biases in the state estimation errors, which may take a quite long time to recover depending on how long the disturbances themselves have affected the filter behavior; the in-line compensation procedure proves to be effective in driving this recovering process. Finally, provided that the time-varying disturbances are detected, the affected measurements from the aiding system are not assimilated in the filtering process, and the orientation sensor relies entirely on the gyro outputs until the next measurement update. An interesting approach which would deserve further investigation is the introduction of a rule to smoothly shift the measurement noise SDs from the initial value to infinity, according to the perceived reliability of the sensed information. For the purpose of this paper, however, we prefer to deflate the adaptation of the measurement noise covariance matrix toward an implementation of gating.

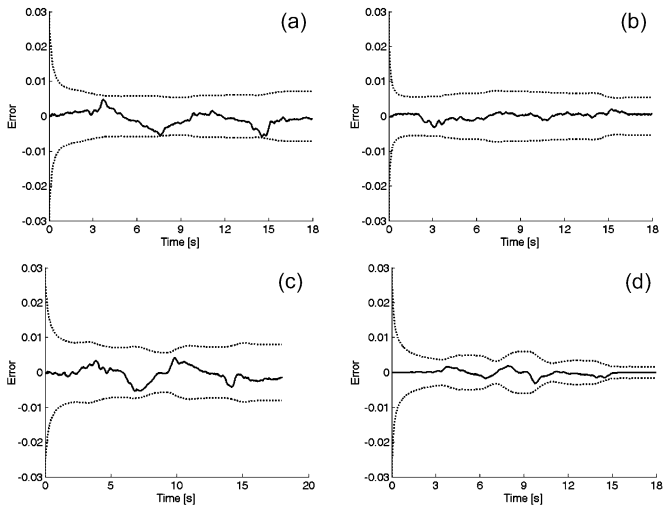

Fig. 4. State errors from the EKF for the four quaternion components (HAND data-set sampled at 100 Hz—method A). The solid lines are the errors and the dotted lines represent the three SD bounds. (a)–(d) First, second, third, fourth quaternion component, respectively.

An additional set of simulations, the results of which are shown in Table IV, is useful to assess the sensitivity of method A to the choice of the random walk model parameters; not surprisingly, it is easy to find other filter parameter initializations,

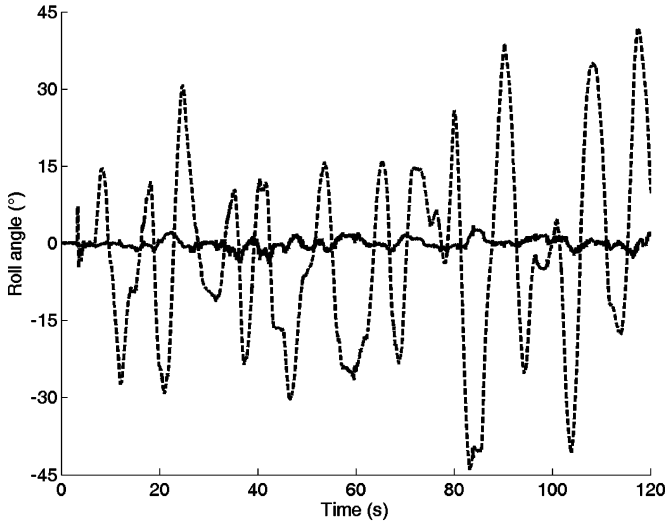

Fig. 5. Time function of the roll angle measured from the Vicon system (truth reference) and the roll angle estimation error, computed as the difference between the roll angle estimate produced by the EKF (Method A) and the truth reference. Dashed line: truth reference, solid line: estimation error.

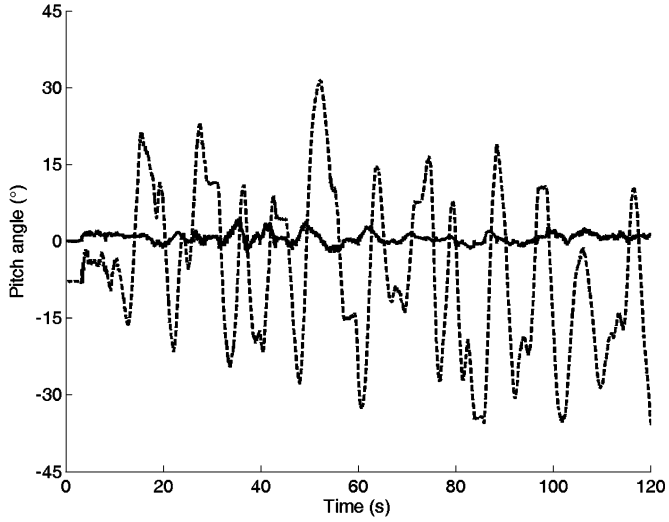

Fig. 6. Time function of the pitch angle measured from the Vicon system (truth reference) and the pitch angle estimation error, computed as the difference between the pitch angle estimate produced by the EKF (Method A) and the truth reference. Dashed line: truth reference, solid line: estimation error.

characterized in particular by smaller values of the random walk SD, which yield better performance in the absence of the disturbances (row named A1); however, when the disturbances are introduced in the simulation (row named A2), this parameter setting turns out to be not well suited, because of the reduced ability of the algorithm to protect against destabilizing effects of the disturbances before their detection occurs.

Within the limits of our analysis, the effect of the sampling rate is not prominent. This is interesting, since the EKF linearization may lead to filter instability unless suitably small sampling intervals are used [28], [30]. It is likely that human motion dynamics is not particularly challenging to track, as discussed at length in [30]. On the other hand, the analysis in [30] is carried out without dealing with the problem of sensor accuracy. It remains to see whether the claim is valid when the estimation task, in the presence of serious measurement errors as investigated in this paper, is extended from orientation components to position components, which require double integration of gravity-compensated acceleration components, or when the estimation task is connected with potentially more challenging human motion dynamics, such as walking. In our recent work on foot inertial sensing for estimating temporo-spatial parameters of gait [21], [24], it is shown that limitations in the sampling frequency can be tolerated down to 25–50 Hz, provided that strap-down integrals can be reliably reset once in a gait cycle [21]; we also demonstrate that the effect of low-frequency errors, e.g., bias and scale factor drifts, is more relevant than the effect of high-frequency errors, e.g., sensor jolting, impact spikes and so forth, which can be accommodated by careful sensor placement and signal filtering [24]. Using relatively slow hand motion signals, as done in the present paper, presents a challenge to the developed quaternion-based EKF, mainly because of the duration of the strap-down integration.

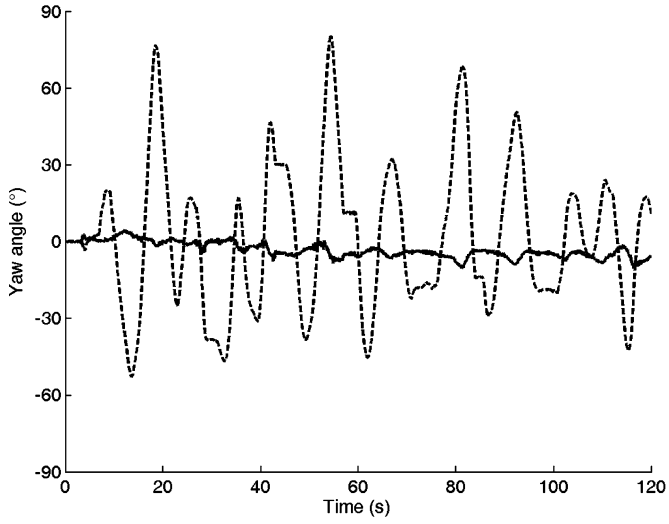

Fig. 7. Time function of the yaw angle measured from the Vicon system (truth reference) and the yaw angle estimation error, computed as the difference between the yaw angle estimate produced by the EKF (Method A) and the truth reference. Dashed line: truth reference, solid line: estimation error.

Within the limits of the experimental validation, the performances of inertial/magnetic sensing are remarkable as compared with those of a state-of-the-art motion capture system. The performance characteristics of the InertiaCube2 are specified by the manufacturer as 1° RMS (static accuracy) and 3° RMS (dynamic accuracy). These specifications are in the same order as those reported for other commercially available MODS products. It comes as no surprise that, in dynamic conditions, the accuracy is generally worse than in static conditions: this is partly because accelerometers, exposed to both gravity and body accelerations, can estimate inclination with limited accuracy. Irrespective of the measurement protocols devised by manufacturers to specify the accuracy of their products, which would also include environment and motion trajectories, inertial sensing for orientation determination does not have a competitive edge over digital optical systems, when the latter technology is not subject to, e.g., line-of-sight or working volume limitations [31]. For the purpose of the experimental validation performed in this paper, the orientation information provided

by a digital optical system such as Vicon can be considered the truth reference for filtering algorithm assessment.

Although all gyros in our sensing hardware appear to work properly, the pitch angle estimation accuracy provided by Method E is unexpectedly poorer as compared with the estimation accuracy of other Euler angles provided by the same method: it is arguable that, because of the time-integration of wideband noise superimposed to gyro signals, the pitch angle estimation accuracy happens to be penalized in this particular experiment. In full compliance with the principles of complementary filtering, however, gravimetric tilt sensing and earth's magnetic field sensing are well suited to stabilize the gyro orientation. It is worthy noting that, while the accuracy of pitch and roll estimates produced by Method A and Method F is similar, the yaw estimate is better when Method A is used. It is not our goal here to compare the developed EKF with the native algorithm within the InertiaCube2, which is simply used here with its default parameter setting. We argue that the improvement of yaw estimate is mainly due to the in-line calibration procedure, and indeed the yaw estimate produced by Method A is about the same order of accuracy as the yaw estimate produced by Method E. A key factor for exploiting the improvement provided by Method A is that the gyro performs reasonably well. The improved EKF promotes a sort of sensor bootstrap: the sensor is forced to rely on itself in order to compensate for the bias drift, since external sensors, e.g., GPS are not used to make the system error states observable. It is, thus, important, for instance, that the gyro bias is captured by zero attitude updates, before bias becomes a dominant factor in determining the orientation uncertainty, which may happen in practice in less than few minutes with commercial grade gyros [1]. Provided that the bias capture feature is active, it is then important that the filter mechanization is studied to prevent the errors incurred by the aiding sensors from degrading the orientation estimator performance.

We have developed an improved quaternion based EKF for estimating the orientation of a rigid body using a MODS endowed with one tri-axis gyro, one tri-axis accelerometer and one tri-axis magnetometer. The EKF incorporates an in-line calibration procedure for modeling time-varying biases which may affect sensors like accelerometers and magnetometers, and a mechanism for adapting their measurement noise covariance matrix in the presence of motion and magnetic disturbances. These two features in combination prove helpful to enhance the accuracy of orientation estimates, as demonstrated by computer simulations and experimental validation in connection with the use of state-of-the-art MODS.

ACKNOWLEDGMENT

The author would like to thank Dr. L. Grimaldi for performing the experimental validation with the Vicon system, and Dr. A. Ravaschio for the assistance in operating this system.

REFERENCES

[1] E. Foxlin, "Motion tracking requirements and technologies," in *Handbook of Virtual Environment Technologies*, K. Stanney, Ed.. Hillsdale, NJ: Lawrence Erlbaum, 2002, ch. 8, pp. 163–210.

[2] C. Verplaetse, "Inertial proprioceptive devices: self-motion-sensing toys and tools," *IBM Syst. J.*, vol. 35, no. 3–4, pp. 639–650, 1996.

[3] M. J. Caruso, "Applications of magnetic sensors for low cost compass systems," in *Proc. IEEE Position, Location and Navigation Symp.*, San Diego, CA, March 13–16, 2000, pp. 177–184.

[4] B. Kemp, A. J. M. W. Janssen, and B. van der Kamp, "Body position can be monitored in 3D using accelerometers and earth-magnetic field sensors," *Electroencephalogr. Clin. Neurophysiol.*, vol. 109, pp. 484–488, 1998.

[5] A. M. Sabatini, "Inertial sensing in biomechanics: a survey of computational techniques bridging motion analysis and personal navigation," in *Computational Intelligence for Movement Sciences: Neural Networks, Support Vector Machines and Other Emerging Techniques*, R. K. Begg and M. Palaniswami, Eds. Hershey, PA: Idea Group Inc., 2006, ch. 2, pp. 70–100.

[6] H. J. Luinge and P. H. Veltink, "Inclination measurement of human movement using a 3-D accelerometer with autocalibration," *IEEE Trans. Neural Syst. Rehab. Eng.*, vol. 12, no. 1, pp. 112–121, Jan. 2004.

[7] J. L. Marins, X. Yun, E. R. Bachmann, R. B. McGhee, and M. J. Zyda, "An extended Kalman filter for quaternion-based orientation estimation using MARG sensors," in *Proc. IEEE/RSJ Int. Conf. Intelligent Robots and Systems* , Mani, HI, Oct. 29–Nov. 03 2001, pp. 2003–2011.

[8] J. C. K. Chou, "Quaternion kinematic and dynamic differential equations," *IEEE Trans. Robot. Autom.*, vol. 8, no. 1, pp. 53–64, 1992.

[9] C. Kirtley, "Summary: Quaternions vs. Euler angles," BIOMCH-L Discussion May 3, 2001 [Online]. Available: http://isb.ri.ccf.org/biomch-l/archives/biomch-l-2001-05

[10] D. Gebre-Egziabher, G. H. Elkaim, J. D. Powell, and B. W. Parkinson, "A gyro-free quaternion-based attitude determination system suitable for implementation using low cost sensors," in *Proc. IEEE Position, Location and Navigation Symp.*, San Diego, CA, Mar. 13–16, 2000, pp. 185–192.

[11] E. Foxlin, M. Harrington, and Y. Altshuler, "Miniature 6-DOF inertial system for tracking HMDs," *Proc. SPIE*, vol. 3362, Aerosense 98, pp. 1–15, 1998.

[12] InterSense, Inc., [Online]. Available: http://www.isense.com/products/prec/ic2/inde x.htm

[13] H. Rehbinder and X. Hu, "Drift-free attitude estimation for accelerated rigid bodies," in *Proc. IEEE Int. Conf. Robotics Automation*, Seoul, Korea, May 21–26, 2001, pp. 4244–4249.

[14] T. Harada, H. Uchino, T. Mori, and T. Sato, "Portable absolute orientation estimation device with wireless network under accelerated situation," in *Proc. IEEE Int. Conf. Robotics Automat.*, New Orleans, LA, Apr. 2004, pp. 1412–1417.

[15] Q. Ladetto and B. Merminod, "In step with INS—navigation for the blind, tracking emergency crews," *GPS World*, pp. 30–38, Oct. 2002.

[16] D. Roetenberg, H. J. Luinge, C. T. M. Baten, and P. H. Veltink, "Compensation of magnetic disturbances improves inertial and magnetic sensing of human body segment orientation," *IEEE Trans. Neural Syst. Rehab. Eng.*, vol. 13, no. 3, pp. 395–405, Mar. 2005.

[17] R. Smith, A. Frost, and P. Probert, "Aspects of heading determination via fusion of inclinometer and magnetometer data," in *Proc. Int. Conf. Advanced Robotics*, Monterrey, CA, Jul. 7–9, 1997, pp. 739–744.

[18] B. Hoff and R. Azuma, "Autocalibration of an electronic compass in an outdoor augmented reality system," in *Proc. IEEE/ACM Int. Symp. Augmented Reality*, Münich, Germany, Oct. 5–6, 2000, pp. 159–164.

[19] F. Ferraris, U. Grimaldi, and M. Parvis, "Procedure for effortless in-field calibration of three-axis rate gyros and accelerometers," *Sensors Mater.*, vol. 7, pp. 311–330.

[20] D. Gebre-Egziabher, G. H. Elkaim, J. D. Powell, and B. W. Parkinson, "A non-linear, two-step estimation algorithm for calibrating solid-state strapdown magnetometers," in *Proc. Int. Conf. Integrated Navigation Systems*, St. Petersburg, Russia, May 28–30, 2001, pp. 290–297.

[21] A. M. Sabatini, "Quaternion based strap-down integration method for applications of inertial sensing to gait analysis," *Med. Biol. Eng. Comput.*, vol. 42, pp. 97–105, 2005.

[22] E. Abbott and D. Powell, "Land-vehicle navigation using GPS," *Proc. IEEE*, vol. 87, no. 1, pp. 145–162, Jan. 1999.

[23] R. Williamson and B. J. Andrews, "Detecting absolute human knee angle and angular velocity using accelerometers and rate gyroscopes," *Med. Biol. Eng. Comp.*, vol. 39, pp. 294–302, 2001.

[24] A. M. Sabatini, C. Martelloni, S. Scapellato, and F. Cavallo, "Assessment of walking features from foot inertial sensing," *IEEE Trans. Biomed. Eng.*, vol. 52, no. 3, pp. 486–494, Mar. 2005.

[25] J. Elwell, "Inertial navigation for the urban warrior," *Proc. SPIE*, vol. 3709, pp. 196–204, 1999.

[26] J. C. Lötters, J. Schipper, P. H. Veltink, W. Olthius, and P. Bergveld, "Procedure for in-use calibration of triaxial accelerometers in medical applications," *Sensors Actuators A*, vol. 68, pp. 221–228, 1998.
[27] D. Choukroun, "Novel methods for attitude determination using vector observations," Ph.D. thesis, Technion, Israel Inst. Technol., Haifa, Israel, 2003.
[28] P. S. Maybeck, *Stochastic Models, Estimation and Control*. New York: Academic, 1979.
[29] J. E. Bortz, "A new mathematical formulation for strapdown inertial navigation," *IEEE Trans. Aerosp. Elec. Syst.*, vol. AES-7, no. 1, pp. 61–66, Jan. 1971.
[30] J. J. LaViola, Jr., "A comparison of unscented and extended Kalman filtering for estimating quaternion motion," in *Proc. American Control Conf.*, Denver, CO, June 4–6, 2003, pp. 2435–2440.
[31] G. Welch and E. Foxlin, "Motion tracking: no silver bullet, but a respectable arsenal," *IEEE Comput. Graphic. Applicat.*, vol. 22, no. 6, pp. 24–38, Nov.–Dec. 2002.

Angelo M. Sabatini (M'90–SM'06) received the Dr. Eng. degree in electrical engineering from the University of Pisa, Pisa, Italy, in 1986, and the Ph.D. degree in biomedical robotics from Scuola Superiore Sant'Anna, Pisa, in 1992.

From 1987–1988 he was with Centro E. Piaggio, Faculty of Engineering, University of Pisa. During the summer of 1988, he was a Visiting Scientist at the Artificial Organ Lab, Brown University, Providence, RI. From 1991–2001, he was an Assistant Professor of Biomedical Engineering at Scuola Superiore Sant'Anna, where he has been an Associate Professor of Biomedical Engineering since 2001. His main research interests are the design and validation of intelligent assistive devices and wearable sensor systems, biomedical signal processing, and quantification of human performance.